Electronic Research Archive

ERA, 31(10): 6236–6259.
DOI: 10.3934/era.2023316
Received: 26 June 2023
Revised: 20 August 2023
Accepted: 11 September 2023
Published: 20 September 2023

http://www.aimspress.com/journal/ERA

*Research article*

# Synchronizability of multilayer star-ring networks with variable coupling strength

**Shuang Liu[1,*], Bigang Xu[1], Qingyun Wang[2] and Xia Tan[1]**

[1] Shanghai Engineering Research Center of Physical Vapor Deposition (PVD) Superhard Coating and Equipment, Shanghai Institute of Technology, Shanghai 201418, China
[2] Department of Dynamics and Control, Beihang University, Beijing 100191, China

* **Correspondence:** Email: lsbbsh@126.com.

**Abstract:** We investigate the synchronizability of multilayer star-ring networks. Two types of multilayer networks, including aggregated coupling and divergent coupling, are established based on the connections between the hub node and the leaf nodes in the subnetwork. The eigenvalue spectrum of the two types of multilayer networks is strictly derived, and the correlation between topological parameters and synchronizability is analyzed by the master stability function framework. Moreover, the variable coupling strength has been investigated, revealing that it is significantly related to the synchronizability of the aggregated coupling while having no influence on the divergent coupling. Furthermore, the validity of the synchronizability analysis is obtained by implementing adaptive control on the multilayer star-ring networks previously mentioned. Calculations and comparisons show that the differences caused by the sizes of multilayer networks and interlayer coupling strength are not negligible. Finally, numerical examples are also provided to validate the effectiveness of the theoretical analysis.

**Keywords:** multilayer networks; synchronizability; eigenvalue spectrum; coupling strength; time-varying topology

## 1. Introduction

Complex networks are extensively explored in the field of nonlinear dynamics [1–3]. Most of the previous studies of networks have focused on single-layer networks, while many real-world networks

cannot be described specifically by single-layer networks alone. With advancements in theory and practice, it has gradually been found that networks do not isolate entities but rather interact with other networks in structure and function. For example, transportation networks [4] are composed of aviation networks, shipping networks and railway networks. The biological networks [5] consist of gene regulatory networks, metabolic networks and protein interaction networks. Therefore, it is imperative to study the multilayer networks formed by the interaction between each single-layer network in depth. It can be abstracted into a multilayer network model with intralayer and interlayer coupling to better interpret the association between sub-networks in the complex relationship. Recent research on multilayer networks has attracted some attention. Zhang et al. [6] studied the adaptive explosive synchronization of multilayer networks without considering the specific correlation between the oscillators and the natural frequency. Wang et al. [7] considered the nodes with Lur'e-type dynamics and investigated how to achieve synchronization from node to whole network in a directional topology. A series of studies have also been carried out in the field of topology identification for multilayer networks. Liu et al. [8] realized topology identification of the networks based on adaptive observers of chaotic external signals without complex linear independence assumptions. Different from previous research strategies, Mei et al. [9] studied the structure identification problem based on the compressed sensing method. In addition, in the study of multilayer network dynamics, Wang et al. [10] investigated the unique superdiffusion phenomenon caused by the directionality of connections. Turalska et al. [11] proved that the correlation existing in the networks would affect the dynamic cascade process and could prevent the spread of failures between layers. Therefore, it is imperative to undertake further exploration of multilayer networks.

Synchronization is a typical topic for the numerous dynamic behaviors observed in complex networks. It plays a significant role in various domains such as multi-agent cooperation, biological oscillators, signal transmission and numerous other applications [12–15]. In 1990, Pecora and Carroll [16] first proposed synchronization control for two coupled chaotic oscillators. Subsequently, the synchronization problems of single-layer complex networks are studied one after another. Wu et al. [17] investigated the phenomenon of projective synchronization in drive-response networks involving complex-variable chaotic systems. Hong et al. [18] researched the phenomenon of collective synchronization in a system of coupled oscillators that were organized on small-world networks. Li et al. [19] employed linear matrix inequalities to examine the synchronization issue in complex dynamical networks with time-varying delays. Due to the complexity of multilayer networks, some methods of synchronization in single-layer networks are no longer applicable. Currently, some advances have been achieved in the field of synchronization research in multilayer networks. Zhao et al. [20] focused on the synchronization of multiplex delayed networks with stochastic perturbations via pinning control, which significantly improved the synchronization efficiency. Fan et al. [21] delved into the study of adaptive event-triggered prescribed performance learning synchronization for complex dynamical networks. The above studies focused on the synchronization of chaotic systems and networks with given topological parameters and coupling strengths. However, the relationship between topological parameters, the size of parameters and coupling strengths changing with time to synchronizability analysis is not clear, which is a challenging task in multilayer networks that deserves further research.

In large-scale complex systems, individual behavior tends to be consistent, which is an external manifestation of synchronizability, and it is very important to understand its influence from the perspective of topology. A supra-Laplacian matrix based on the diffusion dynamics equation of

multilayer networks is proposed to analyze its eigenvalue spectrum for studying complex network synchronizability [22–24]. So far, there have been some initial findings in the study of synchronizability in multilayer complex networks. Aguirre et al. [25] investigated the impact of node degree on the synchronization ability of two interconnected networks. They demonstrated that linking high-degree nodes in each network is the most effective approach for achieving synchronization. The two-layer star networks were derived strictly from the eigenvalue spectrum and analyzed for synchronizability by Xu et al. [26]. Li [27] proposed a two-layer dumbbell network model to analyze the synchronizability and verified the synchronization through a simple numerical simulation. Deng et al. [28] researched the synchronizability of multilayer chain networks. However, in real-world complex networks, whether they are single-layer or multilayer, studying the synchronizability of networks with weighted, directed and variable coupling strength is more meaningful. Variable coupling strength plays an important role in information transmission and complex system control. Adjusting its size can effectively optimize traffic flow regulation and signal coordination in the intelligent transportation system [29]. In the Internet of Things, its regulation can optimize the transmission and processing of information, enabling intelligent detection and control [30]. Given its extensive application in engineering, it cannot be ignored in synchronization analysis. Therefore, apart from considering the influence of topological parameters, we also focus on analyzing the influence of variable coupling strengths on the synchronizability of the network. The common control methods in complex networks include adaptive control, sliding mode control, impulsive control and so on [31,32]. Compared with other methods, the adaptive control strategy selected in this paper has the advantages of adjusting changes independently with network uncertainties, improving the efficiency of synchronization control, and having stronger robustness [33]. Shi et al. [34] realized finite/fixed-time synchronization of complex networks with uncertain internal coupling based on the quantitative adaptive control method. Qin et al. [35] used an adaptive control strategy to study the robust $H_\infty$ synchronization problem of complex networks with multiple delays.

Inspired by the previous literature, we will examine two types of directed multilayer variable coupling strength star-ring networks: divergent coupling and aggregated coupling. In the case of divergent coupling, the hub node establishes connections directed toward the leaf nodes, thus forming a unidirectional communication flow, which plays an important role in improving the reliability and resource coordination of the sensor system [36]. Conversely, aggregated coupling involves the leaf nodes directing connections toward the hub nodes, with advantages such as multi-source data aggregation and resource optimization [37,38]. The major contributions of this paper can be summarized as follows:

(i) The eigenvalue spectrum of the multilayer networks with divergent and aggregated coupling is strictly derived.

(ii) The correlation between topological parameters and synchronizability is analyzed with bounded and unbounded synchronous regions.

(iii) The variable coupling strength in divergent and aggregated coupling star-ring networks has been investigated, which is only related to the synchronizability of the aggregated coupling mode.

The remaining sections of the paper are organized as follows. In Section 2, several preliminaries are provided to establish a foundation for the subsequent discussions. The synchronizability of multilayer divergent and aggregated directionally coupled star-ring networks under varying coupling is illustrated in detail in Sections 3 and 4, respectively. To validate the accuracy of our synchronizability analysis, synchronization controls are provided in Section 5. Finally, in Section 6, we summarize our

conclusions and provide a brief discussion of future work.

## 2. Preliminaries

Consider a complex multilayer network with $M$ layers and $N$ interconnected nodes in each layer. The evolution of a full network dynamical equation is described as follows [39]:

$$\dot{\boldsymbol{x}}_i^K = f\left(\boldsymbol{x}_i^K\right) + c^K \sum_{j=1}^{N} w_{ij}^K \boldsymbol{H}\left(\boldsymbol{x}_j^K\right) + p\sum_{L=1}^{M} d_i^{KZ} \boldsymbol{\Gamma}\left(\boldsymbol{x}_i^Z\right), \tag{1}$$

where $\boldsymbol{x}_i^K \in \mathcal{R}^N$ denotes the state of the $i$th node in the $K$th subnetwork, and $f(\boldsymbol{x}_i^K)$: $\mathcal{R}^N \to \mathcal{R}^N$ governs a nonlinear function of the nodes, $1 \le i \le N$, $1 \le K, Z \le M$ ($K \ne Z$). $c^K > 0$ is the intralayer coupling strength, and $\boldsymbol{H}(\boldsymbol{x}_j^K)$: $\mathcal{R}^N \to \mathcal{R}^N$ is the inner coupling continuous function of the intralayer. $p > 0$ is the interlayer coupling strength, and $\boldsymbol{\Gamma}(\boldsymbol{x}_i^Z)$: $\mathcal{R}^N \to \mathcal{R}^N$ is the inner continuous coupling function of the interlayer. $\boldsymbol{W}^K = (w_{ij}^K) \in \mathcal{R}^{N\times N}$ represents the coupling weight configuration matrix of the $K$th layer, where $w_{ij}^K$ is defined as follows: if there exists a connection between node $i$ and $j (i \ne j)$ within the $K$th layer, then $w_{ij}^K = w_{ji}^K = 1$; otherwise, $w_{ij}^K = w_{ji}^K = 0$. In addition, the diagonal elements of $\boldsymbol{W}^K$ satisfy the following condition:

$$w_{ii}^K = -\sum\nolimits_{j=1, j\ne i}^{K} w_{ij}^K.$$

Therefore, $\boldsymbol{L}^K = -c^K \boldsymbol{W}^K$ is a Laplacian matrix of the $K$th layer. Similarly, the interlayer weight $d_i^{KZ} = d_i^{ZK} = 1$ if node $i$ in the $K$th layer is connected to node $j$ in the $Z$th layer. Otherwise, $d_i^{KZ} = d_i^{ZK} = 0$. Likewise,

$$d_i^{KK} = -\sum\nolimits_{Z=1, Z\ne K}^{M} d_i^{KZ}, K, Z = 1, 2, \cdots, M.$$

Then, $\boldsymbol{D} = (d_i^{KZ}) \in \mathcal{R}^{M\times M}$ is the negative Laplacian matrix of the interlayer. Let $\boldsymbol{\mathcal{L}}^{\mathrm{L}}$ be the supra-Laplacian matrix that represents the interlayer topology and $\boldsymbol{\mathcal{L}}^{\mathrm{I}}$ be the supra-Laplacian matrix that represents the intralayer topology. Then, the supra-Laplacian matrix of the above system is described as [40]:

$$\boldsymbol{\mathcal{L}} = \boldsymbol{\mathcal{L}}^{\mathrm{I}} + \boldsymbol{\mathcal{L}}^{\mathrm{L}}. \tag{2}$$

Let $\boldsymbol{L}^I$ denote the Laplacian matrix of the interlayer networks. Specifically, the interlayer supra-Laplacian matrix is

$$\boldsymbol{\mathcal{L}}^{\mathrm{I}} = \boldsymbol{L}^{\mathrm{I}} \otimes \boldsymbol{I}_N, \tag{3}$$

where $\otimes$ is the Kronecker product and $\boldsymbol{I}_N$ represents the $N \times N$ identity matrix. The intralayer supra-Laplacian matrix of a multiplex network is defined as:

$$\boldsymbol{\mathcal{L}}^{\mathrm{L}}=\begin{pmatrix} \boldsymbol{L}^1 & 0 & \cdots & 0 \\ 0 & \boldsymbol{L}^2 & \cdots & 0 \\ \vdots & \vdots & \ddots & \vdots \\ 0 & 0 & \cdots & \boldsymbol{L}^M \end{pmatrix}=\bigoplus_{K=1}^{M}\boldsymbol{L}^K, \tag{4}$$

where $K = 1, 2, \ldots, M$, and $\boldsymbol{L}^K$ is the Laplacian matrix of the $K$th layer.

In accordance with the master stability function framework [41], we can analyze whether the eigenvalues of the multilayer network fall in the corresponding synchronous regions to judge the synchronizability of the network. Both bounded and unbounded regions are usually the two main categories for discussion. If the network has an unbounded synchronous region, the minimum nonzero eigenvalue $\lambda_2$ of $\boldsymbol{\mathcal{L}}$ is key to research the synchronizability. Moreover, synchronizability is positively correlated with $\lambda_2$. On the other hand, if the network has a bounded synchronous region, the synchronizability depends on the ratio $R = \lambda_{\max}/\lambda_2$, which is the maximum eigenvalue $\lambda_{max}$ to the minimum nonzero eigenvalue $\lambda_2$ of $\boldsymbol{\mathcal{L}}$. At this time, synchronizability is negatively correlated with $R$.

For the necessity of subsequent theoretical deduction, a lemma and two hypotheses are presented here:

**Lemma 2.1.** *[42] $\boldsymbol{A}$ and $\boldsymbol{B}$ are $N \times N$ matrices, $M$ is the number of layers, then*

$$\begin{vmatrix} \boldsymbol{A} & \boldsymbol{B} & \cdots & \boldsymbol{B} \\ \boldsymbol{B} & \boldsymbol{A} & \cdots & \boldsymbol{B} \\ \vdots & \vdots & \ddots & \vdots \\ \boldsymbol{B} & \boldsymbol{B} & \cdots & \boldsymbol{A} \end{vmatrix}_{M\times M} = \left|\boldsymbol{A}-\boldsymbol{B}\right|^{M-1}\cdot\left|\boldsymbol{A}+(M-1)\boldsymbol{B}\right|. \tag{5}$$

**Hypothesis 2.1.** *[43] Suppose that there exists $\alpha > 0$, $i = 1, 2, \ldots, N$, $K = 1, 2, \ldots, M$, such that*

$$f\left(\boldsymbol{e}_i^K(t)+\boldsymbol{s}(t)\right)-f\left(\boldsymbol{s}(t)\right)\le\alpha\boldsymbol{e}_i^K(t), \tag{6}$$

*where, $\boldsymbol{e}_i^K(t)$ and $\boldsymbol{s}(t)$ represent the synchronization errors and target system of the network, respectively.*

**Hypothesis 2.2.** *[44] For any $\boldsymbol{p}$, $\boldsymbol{q}\in\mathcal{R}^n$, there exists a positive definite matrix $\boldsymbol{Q}\in\mathcal{R}^{n\times n}$, and the following always holds*:

$$\boldsymbol{p}^{\mathrm{T}}\boldsymbol{q}\le\frac{1}{2}\boldsymbol{p}^{\mathrm{T}}\boldsymbol{Q}\,\boldsymbol{p}+\frac{1}{2}\boldsymbol{q}^{\mathrm{T}}\boldsymbol{Q}^{-1}\boldsymbol{q}. \tag{7}$$

## 3. Synchronizability of multilayer network with divergent coupling

Based on the theory of Section 2, a multilayer star-ring network with divergent coupling is constructed, and its characteristic spectrum is strictly derived. Furthermore, when the synchronous region is unbounded or bounded, the influence of different topological parameters on synchronizability is studied in this section.

### *3.1. The structure of the multilayer network with divergent coupling*

In this section, the synchronizability analysis of the divergent directionally coupled star-ring

network is considered, and its topology is shown in Figure 1. The left panel describes the intralayer connection of each subnetwork in the multilayer network, and the right panel shows the one-to-one connection of the subnetwork nodes of each layer. $L^{(1)}$, $L^{(2)}$, …, $L^{(M)}$ represent each layer. Assume that the topologies of each subnetwork are the same. There are $N$ nodes in each subnetwork, and $M$ represents the number of layers. The blue nodes and the red nodes represent the leaf nodes and the hub nodes, respectively. The nodes at each layer are connected one to one. It is assumed that the connections between nodes within a layer exhibit directionality, while the interlayer connections of each subnetwork are undirected. The red nodes all point one way to the blue nodes and the blue node points to the next blue node. In the aggregated coupling network, $d_0$ represents the corresponding coupling strength between each leaf node in each subnetwork. The remaining $d$ represents the coupling strength between each leaf node. The intralayer coupling strength of blue nodes is given by $a_0$. Suppose that the intralayer coupling strength of the red node points to the blue nodes is denoted as $a$ and the total intralayer coupling strength is ($N$-1) $a$ at the initial time. At some time, $\gamma$ ($\gamma$ is even) of coupling strength becomes $\sigma a$, then the coupling strength of the remaining ($N$-$\gamma$-1) nodes becomes ($N$-$\sigma\gamma$-1) $a$/($N$-$\gamma$-1). We have denoted ($N$-$\sigma\gamma$-1) $a$/($N$-$\gamma$-1) as $\delta a$ for convenience.

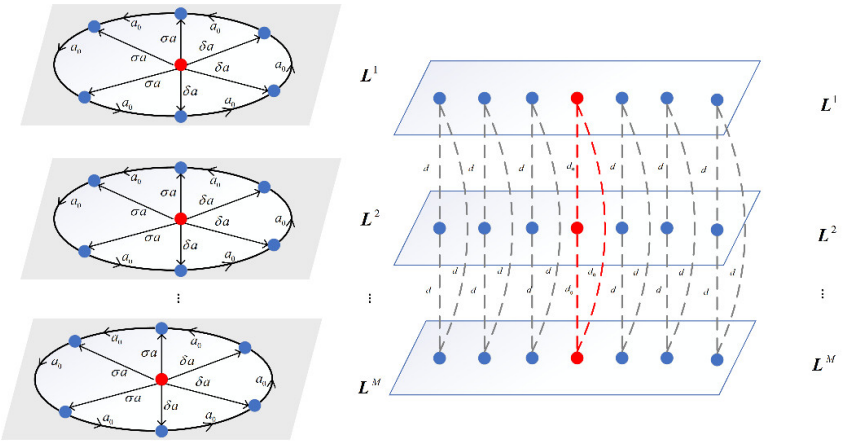

**Figure 1.** Schematic diagram of the multilayer star-ring network with divergent coupling.

### *3.2. The eigenvalue spectrum and synchronizability*

The supra-Laplacian matrix of the network can be written as:

$$\mathcal{L} = \begin{pmatrix} \boxtimes & \boxplus & \cdots & \boxplus \\ \boxplus & \boxtimes & \cdots & \boxplus \\ \vdots & \vdots & \ddots & \vdots \\ \boxplus & \boxplus & \cdots & \boxtimes \end{pmatrix}.$$

In detail, $\boxplus = diag\left(-d_0, -d, -d, \cdots, -d\right)_{N\times N}$, and

$$\text{❷}=\begin{pmatrix}(M-1)d_0+(N-1)a & -\sigma a & -\sigma a & \cdots & -\sigma a & -\delta a & \cdots & -\delta a\\ 0 & (M-1)d+a_0 & 0 & \cdots & 0 & 0 & \cdots & -a_0\\ 0 & -a_0 & (M-1)d+a_0 & \cdots & 0 & 0 & \cdots & 0\\ \vdots & \vdots & \vdots & \ddots & \vdots & \vdots & \ddots & \vdots\\ 0 & 0 & 0 & \cdots & (M-1)d+a_0 & 0 & \cdots & 0\\ 0 & 0 & 0 & \cdots & -a_0 & (M-1)d+a_0 & \cdots & 0\\ \vdots & \vdots & \vdots & \ddots & \vdots & \vdots & \ddots & \vdots\\ 0 & 0 & 0 & \cdots & 0 & 0 & \cdots & (M-1)d+a_0\end{pmatrix}.$$

According to Lemma 2.1, the corresponding characteristic polynomial of $\mathcal{L}$ is expressed as follows:

$$\begin{aligned}|\lambda I-\mathcal{L}|=&\left[\lambda-Md_0-(N-1)a\right]^{M-1}\left[(-1)^N a_0{}^{N-1}+(\lambda-Md-a_0)^{N-1}\right]^{M-1}\\ &\cdot\left[\lambda-(N-1)a\right]\left[(-1)^{2+N}a_0{}^{N-1}+(\lambda-a_0)^{N-1}\right].\end{aligned}$$

From the characteristic polynomial above, whether the topological parameter $N$ is odd or even affects the eigenvalues, which will be discussed below.

**Table 1.** $\lambda_2$ and $R$ change with $N$, $a$, $a_0$, $d$, $d_0$, and $M$ when $N$ is odd or even.

| | | $N\uparrow$ | $a\uparrow$ | $a_0\uparrow$ | $d\uparrow$ | $d_0\uparrow$ | $M\uparrow$ |
|---|---|---|---|---|---|---|---|
| $N$ is odd | $\lambda_2=2a_0$ | — | — | ↑ | — | — | — |
| | $R=(Md_0+(N\text{-}1)\,a)/2a_0$ | ↑ | ↑ | ↓ | — | ↑ | ↑ |
| $N$ is even | $\lambda_2=Md$ | — | — | — | ↑ | — | ↑ |
| | $R=(Md_0+(N\text{-}1)\,a)/Md$ | ↑ | ↑ | — | ↓ | ↑ | ↓ |

—: Unchange; ↑: Increase; ↓: Decrease.

**Table 2.** Synchronizability changes with $N$, $a$, $a_0$, $d$, $d_0$, and $M$ when $N$ is odd or even.

| | | | $N\uparrow$ | $a\uparrow$ | $a_0\uparrow$ | $d\uparrow$ | $d_0\uparrow$ | $M\uparrow$ |
|---|---|---|---|---|---|---|---|---|
| $N$ is odd | *Unbounded* | $\lambda_2=2a_0$ | — | — | ↑ | — | — | — |
| | *Bound* | $R=(Md_0+(N\text{-}1)\,a)/2a_0$ | ↓ | ↓ | ↑ | — | ↓ | ↓ |
| $N$ is even | *Unbounded* | $\lambda_2=Md$ | — | — | — | ↑ | — | ↑ |
| | *Bound* | $R=(Md_0+(N\text{-}1)\,a)/Md$ | ↓ | ↓ | — | ↑ | ↓ | ↑ |

—: Unchange; ↑: Strengthened; ↓: Weakened.

1) $N$ is odd, the eigenvalues $\mathcal{L}$ are:

$$\lambda=\underbrace{0,\cdots,0}_{(N-1)/2},\underbrace{2a_0,\cdots,2a_0}_{(N-1)/2},(N-1)a,\underbrace{Md,\cdots,Md}_{((N-1)/2)(M-1)},\underbrace{Md+2a_0,\cdots,Md+2a_0}_{((N-1)/2)(M-1)},\underbrace{Md_0+(N-1)a,\cdots,Md_0+(N-1)a}_{M-1}.$$

Where, 0 and $2a_0$ are $(N\text{-}1)/2$ multiple roots, $Md$ and $Md+2a_0$ are $((N\text{-}1)/2)$ $(M\text{-}1)$ multiple roots, and $Md_0+(N\text{-}1)\,a$ are $M\text{-}1$ multiple roots, respectively. Due to the fact that $Md >> 2a_0$, thus $\lambda_2=2a_0$, $\lambda_{\max}=Md_0+(N\text{-}1)\,a$, $R=\lambda_{\max}/\lambda_2=(Md_0+(N\text{-}1)\,a)/2a_0$.

2) $N$ is even, the eigenvalues $\mathcal{L}$ are:

$$\lambda = \underbrace{0,\cdots,0}_{(N-1)},\underbrace{Md,\cdots,Md}_{(N-1)(M-1)},(N-1)a,\underbrace{Md_0+(N-1)a}_{M-1}.$$

Both 0, $Md$, and $Md_0$+($N$-1) $a$ are multiple roots. As above, $\lambda_2 = Md$, $\lambda_{max} = Md_0$+($N$-1) $a$, and $R = \lambda_{max}/\lambda_2 = (Md_0$+($N$-1) $a)/Md$. It is obvious that $\sigma a$ doesn't affect the synchronizability based on the above eigenvalues.

The relationships between $\lambda_2$, $R$, and the topological parameters are depicted in Table 1. Similarly, Table 2 presents the correlations between the network's synchronizability and its topological parameters.

### *3.3. Comparisons and discussions*

Numerical experiments between topological parameters and $\lambda_2$, $R$ of multilayer networks will be investigated. That is, including $N$, $a$, $a_0$, $d$, $d_0$, and $M$ to discuss the synchronizability.

1) Influence of the number of subnetwork nodes $N$

Take $a_0 = 0.6$, $d = 1$, $M = 15$, $d_0 = 0.1$, and $a = 1$ to examine the synchronizability with $N$ ($N$ varies from 9 to 399 if $N$ is odd; $N$ varies from 10 to 400 if $N$ is even). Figure 2(a) shows that $\lambda_2$ doesn't change with $N$ in the subnetwork, that is, the synchronizability is not affected. The relationship between $R$ and $N$ is shown in Figure 2(b), which indicates that synchronizability is negatively correlated with $N$.

2) Influence of the intralayer coupling strength $a$

Take $a_0 = 0.6$, $M = 15$, $d = 1$, $d_0 = 0.1$, $N$ (odd) = 399, and $N$ (even) = 400 to examine the synchronizability with $a$. As is shown in Figure 3(a), $\lambda_2$ is unchanged with $a$, that is, the synchronizability is also unchanged with $a$. Then Figure 3(b) displays the relationships between $R$ and $a$, which means that synchronizability is negatively correlated with $a$.

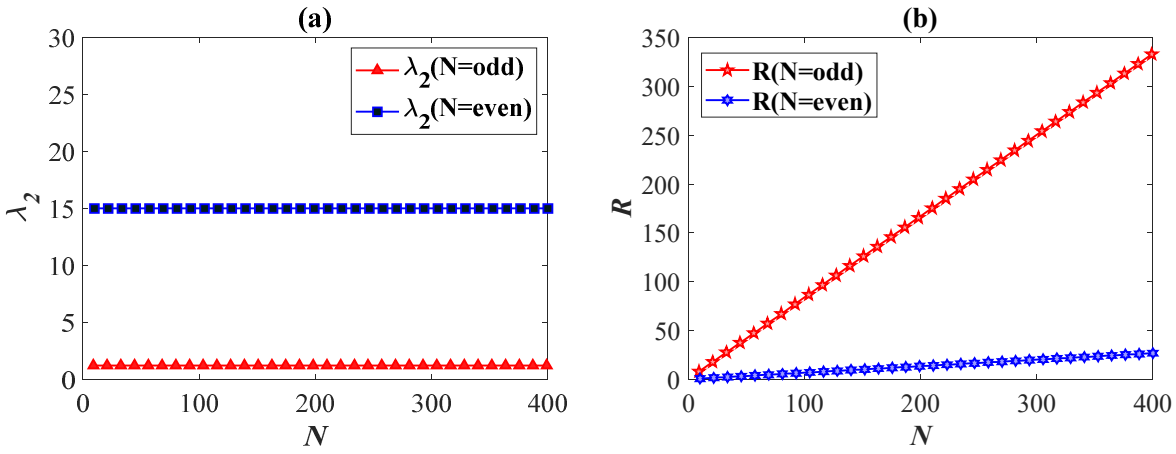


**Figure 2.** $\lambda_2$ and $R$ of the divergent coupled star-ring network change with $N$.

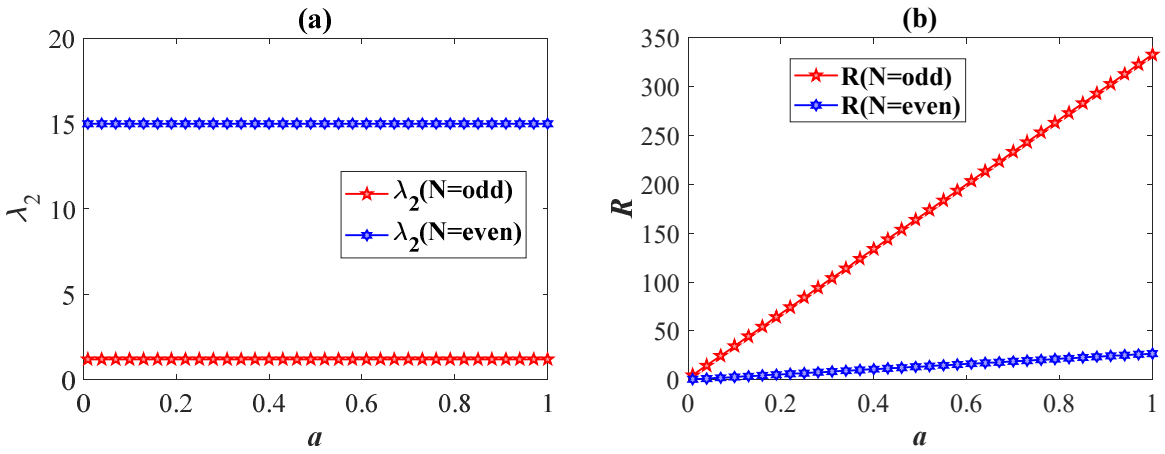


**Figure 3.** $\lambda_2$ and $R$ of the divergent coupled star-ring network change with $a$.

3) Influence of the intralayer coupling strength $a_0$

Take $a$ = 1, $M$ = 15, $d$ = 1, $d_0$ = 0.1, $N$ (odd) = 399, and $N$ (odd) = 400 to explore the synchronizability with $a_0$. Notice from Figure 4(a) that when $N$ is even, $\lambda_2$ unchanged with $a_0$, that is, the synchronizability is not affected. However, when $N$ is odd, $\lambda_2$ exhibits a positive correlation with $a_0$, indicating that a higher value of $a_0$ is associated with increased synchronizability. Notice from Figure 4(b) that when $N$ is even, $R$ remains unchanged, so the synchronizability is not affected. However, $R$ decreases with $a_0$, so the synchronizability strengthens.

4) Influence of the intralayer coupling strength $a_0$

Take $a$ = 1, $a_0$ = 1, $M$ = 15 ($N$ = odd), $M$ = 15, 16, 17 ($N$ = even), $d_0$ = 0.1, $N$ (odd) = 399, and $N$(even) = 400) to explore the synchronizability with $d$. From Figure 5(a), $\lambda_2$ is unchanged with $d$ when $N$ is odd, which means that synchronizability is unchanged. Additionally, $\lambda_2$ increases with $d$ by selecting three group data when $N$ is even, and the synchronizability becomes stronger. From Figure 5(b), $R$ is unchanged with $d$ when $N$ is odd, which means that synchronizability is unchanged. And $R$ decreases with $d$ by selecting three group data when $N$ is even, the synchronizability becomes stronger.

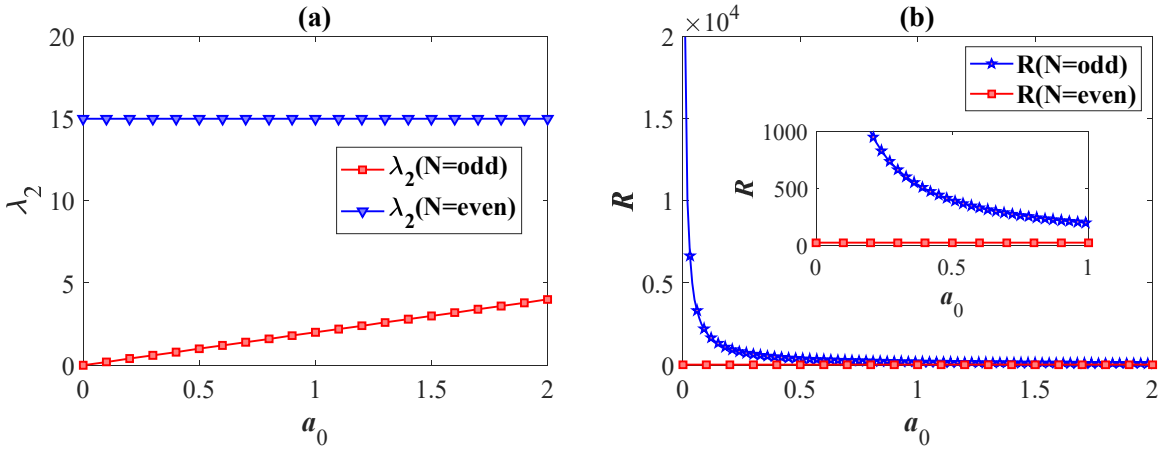


**Figure 4.** $\lambda_2$ and $R$ of the divergent coupled star-ring network change with $a_0$.

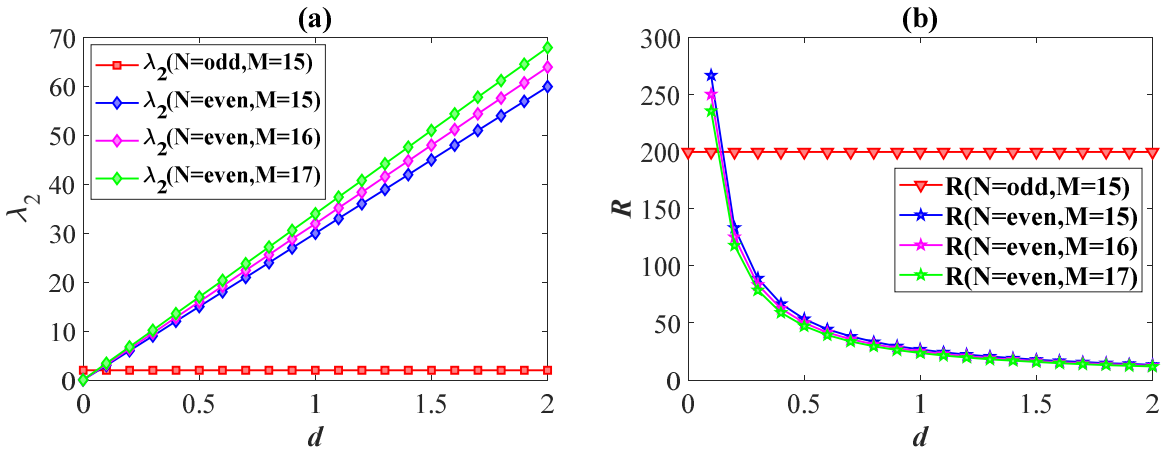


**Figure 5.** $\lambda_2$ and $R$ of the divergent coupled star-ring network change with $d$.

5) Influence of the interlayer coupling strength $d_0$

Take $a = 1$, $a_0 = 1$, $M = 15$, $d = 1$, $N$ (odd) = 399, and $N$ (even) = 400 to study the synchronizability with $d_0$. Figure 6(a) clearly indicates that $\lambda_2$ is not affected by the change of $d_0$, that is, the synchronizability is stable. As is shown in Figure 6(b), $R$ increases with $d_0$. It is revealed that the greater the coupling strength $d_0$, the less favorable the synchronizability.

6) Influence of the number of layers $M$

Take $a = 1$, $a_0 = 1$, $d = 1$ ($N$ = odd), $d = 1$, 1.3, 1.6 ($N$ = even), $N$ (odd) = 399, and $N$ (even) = 400 to analyze the synchronizability with $M$. Figure 7(a) shows that $\lambda_2$ is unchanged with $M$ when $N$ is odd, which means the synchronizability is unchanged. Additionally, $\lambda_2$ increases with the $M$ by selecting three group data, when $N$ is even, the synchronizability becomes stronger with the $M$. Figure 7(b) shows that $R$ increases slowly with $M$ when $N$ is odd, and then the synchronizability decreases. And $R$ decreases with $M$ when $N$ is even; the synchronizability strengthens with $M$.

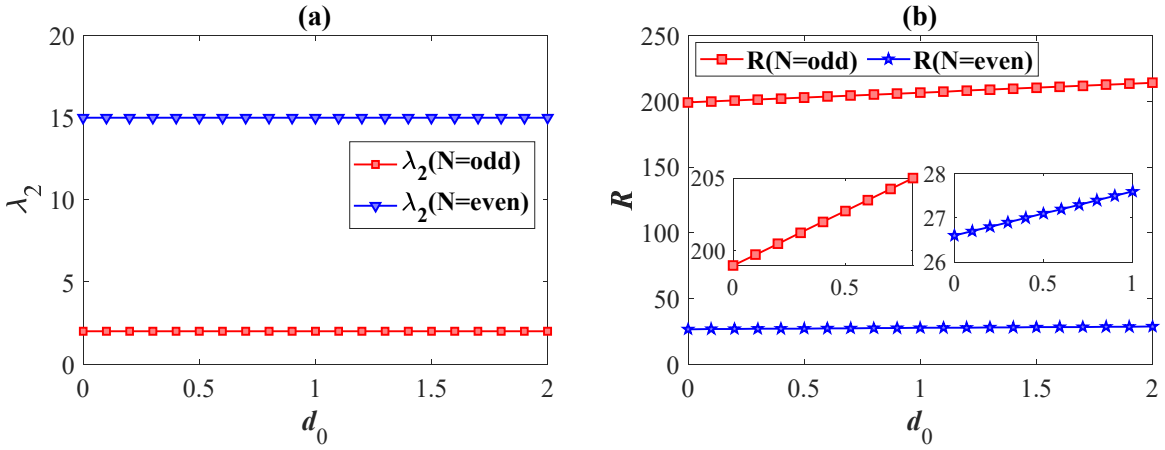


**Figure 6.** $\lambda_2$ and $R$ of the divergent coupled star-ring network change with $d_0$.

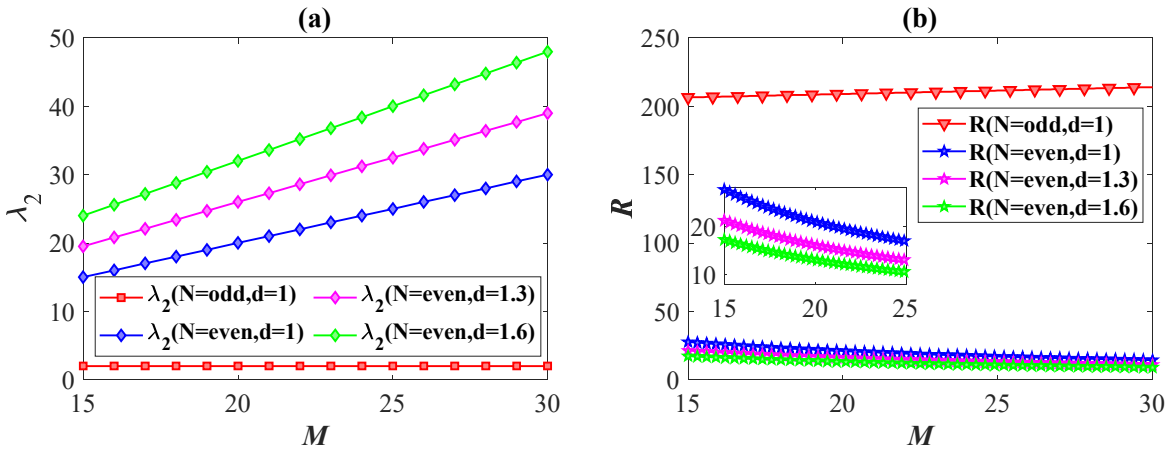


**Figure 7.** $\lambda_2$ and $R$ of the divergent coupled star-ring network change with $M$.

## 4. Synchronizability of multilayer network with aggregated coupling

In contrast to the divergent coupling, a multilayer star-ring network with aggregated coupling is built. In addition, the characteristic spectrum of the network is rigorously derived. Through theoretical deduction, we find that variable coupling strength has a significant influence on synchronizability, except for topological parameters. Furthermore, the influence of variable coupling strength on synchronizability under different function variation rules is discussed in this section.

### *4.1. The structure of the multilayer network with aggregated coupling*

We consider an aggregated directionally coupled star-ring network as shown in Figure 8. Only, unlike the topology of Figure 1, the blue nodes all point to the red nodes within each layer.

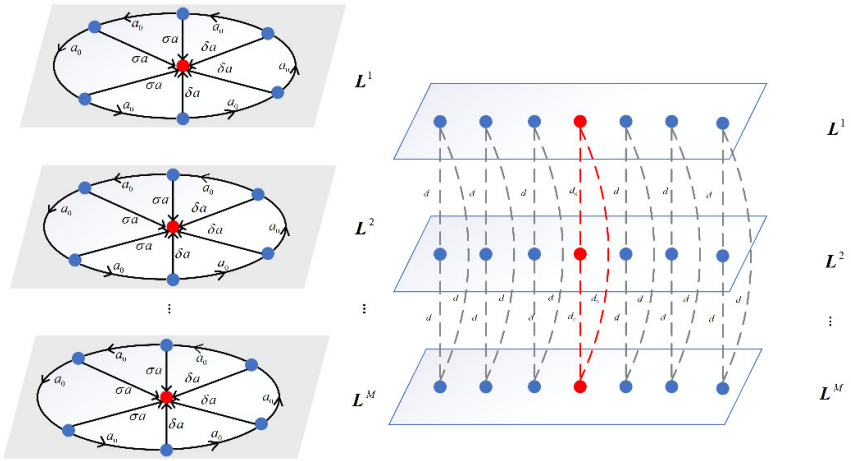


**Figure 8.** Schematic diagram of the multilayer star-ring network with aggregated coupling.

*4.2. The eigenvalue spectrum and synchronizability*

The supra-Laplacian matrix of the network can be written as:

$$\mathcal{L}=\begin{pmatrix} \mathbf{\Omega} & \mathbf{\Xi} & \cdots & \mathbf{\Xi} \\ \mathbf{\Xi} & \mathbf{\Omega} & \cdots & \mathbf{\Xi} \\ \vdots & \vdots & \ddots & \vdots \\ \mathbf{\Xi} & \mathbf{\Xi} & \cdots & \mathbf{\Omega} \end{pmatrix}.$$

In detail, $\mathbf{\Xi}=diag\left(-d_0,-d,-d,\cdots,-d\right)_{N\times N}$, and

$$\mathbf{\Omega}=\begin{pmatrix} (M-1)d_0 & 0 & 0 & \cdots & 0 & 0 & \cdots & 0 \\ -\sigma a & (M-1)d+\sigma a+a_0 & 0 & \cdots & 0 & 0 & \cdots & -a_0 \\ -\sigma a & -a_0 & (M-1)d+\sigma a+a_0 & \cdots & 0 & 0 & \cdots & 0 \\ \vdots & \vdots & \vdots & \ddots & \vdots & \vdots & \ddots & \vdots \\ -\sigma a & 0 & 0 & \cdots & (M-1)d+\sigma a+a_0 & 0 & \cdots & 0 \\ -\delta a & 0 & 0 & \cdots & -a_0 & (M-1)d+\delta a+a_0 & \cdots & 0 \\ \vdots & \vdots & \vdots & \ddots & \vdots & \vdots & \ddots & \vdots \\ -\delta a & 0 & 0 & \cdots & 0 & 0 & \cdots & (M-1)d+\delta a+a_0 \end{pmatrix}.$$

According to Lemma 2.1, the corresponding characteristic polynomial $\mathcal{L}$ is expressed as follows:

$$\begin{aligned} \left|\lambda I-\mathcal{L}\right| =& \lambda\left[\left(-1\right)^{2+N}{a_0}^{N-1}+\left(\lambda-\sigma a-a_0\right)^{\gamma}+\left(\lambda-\delta a-a_0\right)^{N-\gamma-1}\right]^{M-1} \\ & \cdot\left(\lambda-Md_0\right)^{M-1}\left[\left(-1\right)^{2+N}{a_0}^{N-1}+\left(\lambda-Md-\sigma a-a_0\right)^{\gamma}+\left(\lambda-Md-\delta a-a_0\right)^{N-\gamma-1}\right]. \end{aligned}$$

From the characteristic polynomial above, whether the topological parameter $N$ is odd or even affects the eigenvalues, which will be discussed below.

1) $N$ is odd, the eigenvalues of $\mathcal{L}$ are:

$$\lambda=0,\underbrace{Md_0,\cdots,Md_0}_{M-1},\underbrace{\sigma a,\cdots,\sigma a}_{(\gamma/2)(M-1)},\underbrace{\sigma a+2a_0,\cdots,\sigma a+2a_0}_{(\gamma/2)(M-1)},\underbrace{\delta a,\ldots\delta a}_{((N-\gamma-1)/2)(M-1)},\underbrace{\delta a+2a_0,\cdots,\delta a+2a_0}_{((N-\gamma-1)/2)(M-1)},\underbrace{Md+\sigma a,\cdots,Md+\sigma a}_{(\gamma/2)(M-1)},$$
$$\underbrace{Md+\sigma a+2a_0,\cdots,Md+\sigma a+2a_0}_{(\gamma/2)(M-1)},\underbrace{Md+\delta a,\cdots,Md+\delta a}_{((N-\gamma-1)/2)(M-1)},\underbrace{Md+\delta a+2a_0,\cdots,Md+\delta a+2a_0}_{((N-\gamma-1)/2)(M-1)}.$$

Where, $Md_0$ is $M$-1 multiple roots, $\sigma a$, $\sigma a$+2$a_0$, $Md$+$\sigma a$ and $Md$+$\sigma a$+2$a_0$ are ($\gamma$/2) ($M$-1) multiple roots, $\delta a$, $\delta a$+2$a_0$, $Md$+$\delta a$ and $Md$+$\delta a$+2$a_0$ are (($N$-$\gamma$-1)/2) ($M$-1) multiple roots. In view of $Md_0$ >> {$\sigma a$, $\delta a$}, thus $\lambda_{max}$ = max {$Md$+$\sigma a$+2$a_0$, $Md$+$\delta a$+2$a_0$}, $\lambda_2$ = min {$\sigma a$, $\delta a$}, $R=\lambda_{max}/\lambda_2$ = max {$Md$+$\sigma a$+2$a_0$, $Md$+$\delta a$+2$a_0$}/min {$\sigma a$, $\delta a$}.

2) $N$ is even, the eigenvalues of $\mathcal{L}$ are:

$$\lambda=0,\underbrace{Md_0,\cdots,Md_0}_{M-1},\underbrace{\sigma a,\cdots,\sigma a}_{\gamma(M-1)},\underbrace{\delta a,\ldots\delta a}_{(N-\gamma-1)(M-1)},\underbrace{Md+\sigma a,\cdots,Md+\sigma a}_{\gamma(M-1)},\underbrace{Md+\delta a,\cdots,Md+\delta a}_{(N-\gamma-1)(M-1)}.$$

Where, $Md_0$ is $M$-1 multiple roots, $\sigma a$ and $Md$+$\sigma a$ are $\gamma$ ($M$-1) multiple roots, $\delta a$ and $Md$+$\delta a$ are ($N$-$\gamma$-1) ($M$-1) multiple roots. In view of $Md_0$ >> {$\sigma a$, $\delta a$}, thus $\lambda_{max}$ = max {$Md$+$\sigma a$, $Md$+$\delta a$}, $\lambda_2$ = min {$\sigma a$, $\delta a$}, $R=\lambda_{max}/\lambda_2$ = max {$Md$+$\sigma a$, $Md$+$\delta a$}/min {$\sigma a$, $\delta a$}.

It is obvious that the variable coupling strengths $\sigma a$ and $\delta a$ will affect the synchronizability from the above eigenvalues. Different from Section 3, the impact of varying coupling strengths $\sigma a$ and $\delta a$

on synchronizability will be investigated in this section.

**Remark 1.** *Compared with the unidirectional connection between the hub node and the leaf nodes in [45], we discuss the influence of topological parameters and variable coupling strength on synchronizability through divergent and aggregated coupling. Moreover, the characteristic spectrum of multilayer divergent and aggregated coupling networks is also accurately obtained. And it is concluded that the topological parameters influencing the synchronizability of the network are different when the directionality of the node connections is changed.*

### *4.3. Comparisons and discussions*

According to the above theoretical derivation, the number of nodes in the subnetwork has no effect on synchronizability. Moreover, $\lambda_2$ and $R$ in the two cases are basically similar, so $N$ is selected as odd for further study. To investigate the network synchronizability under variable coupling strengths $\sigma a$ and $\delta a$, the partial coupling strength is varied. Let the variable coupling strength follow the principles of the proportional function, the inverse proportional function, the exponential function, the logarithmic function, and the trigonometric function, respectively. The principles of variable coupling strength are as follows: $\sigma_1 = t$, $\sigma_2 = 1/t$, $\sigma_3 = 0.9^t$, $\sigma_4 = \lg(t)$, $\sigma_5 = \sin t+1.5$.

1) Variable coupling strength follows the proportional function

We take $\sigma_1 = t$ (then $\delta_1 = (N\text{-}t\gamma\text{-}1)/(N\text{-}\gamma\text{-}1)$) for the numerical simulation. Then, $\lambda_2 = \min\{\sigma_1 a, \delta_1 a\}$, $R = \lambda_{\max}/\lambda_2 = \max\{Md+\sigma_1 a+2a_0, Md+\delta_1 a+2a_0\}/\min\{\sigma_1 a, \delta_1 a\}$. Figure 9(a) shows the coupling strength $a$ versus the proportional function, and the color depth corresponds to the value of $\lambda_2$. If $t$ is fixed, $\lambda_2$ increases with $a$, and synchronizability is improved. If $a$ is fixed, $\lambda_2$ first increases and then decreases with $t$. Obviously, when $t = 1$ and $a = 5$, $\lambda_2$ reaches its maximum and the synchronizability is the strongest. Figure 9(b) shows the coupling strength $a$ versus the proportional function, and the color depth corresponds to the value of $R$. If $t$ is fixed, $R$ decreases with $a$, and synchronizability is improved. Additionally, if $a$ is fixed, $R$ first decreases and then increases as $t$ increases. Obviously, when $t = 1$ and $a = 5$, $R$ reaches its minimum, and the synchronizability is the strongest.

2) Variable coupling strength follows the inverse proportional function

We take $\sigma_2 = 1/t$ (then $\delta_2 = (N\text{-}(1/t)\ \gamma\text{-}1)/(N\text{-}\gamma\text{-}1)$) for the numerical simulation. Then, $\lambda_2 = \min\{\sigma_2 a, \delta_2 a\}$, $R = \lambda_{\max}/\lambda_2 = \max\{Md+\sigma_2 a+2a_0, Md+\delta_2 a+2a_0\}/\min\{\sigma_2 a, \delta_2 a\}$. Figure 10(a) shows the coupling strength $a$ versus the inverse proportional function, and the color depth corresponds to the value of $\lambda_2$. If $t$ is fixed, $\lambda_2$ increases with $a$, and synchronizability is improved. Additionally, if $a$ is fixed, $\lambda_2$ first increases and then decreases with $t$. Obviously, when $t = 1$ and $a = 5$, $\lambda_2$ reaches its maximum, and the synchronizability is the strongest. Figure 10(b) shows the coupling strength $a$ versus the inverse proportional function, and the color depth corresponds to the value of $R$. If $t$ is fixed, $R$ decreases with $a$, and synchronizability is improved. Additionally, if $a$ is fixed, $R$ first decreases and then increases as $t$ increases. Obviously, when $t = 1$ and $a = 5$, $R$ reaches its minimum, and the synchronizability is the strongest.

3) Variable coupling strength follows the exponential function

We take $\sigma_3 = 0.9^t$ (then $\delta_3 = (N\text{-}(0.9^t)\ \gamma\text{-}1)/(N\text{-}\gamma\text{-}1)$) for the numerical simulation. Then $\lambda_2 = \min\{\sigma_4 a, \delta_4 a\}$, $R = \lambda_{\max}/\lambda_2 = \max\{Md+\sigma_4 a+2a_0, Md+\delta_4 a+2a_0\}/\min\{\sigma_4 a, \delta_4 a\}$. Then $\lambda_2 = \min\{\sigma_4 a, \delta_4 a\}$, $R = \lambda_{\max}/\lambda_2 = \max\{Md+\sigma_4 a+2a_0, Md+\delta_4 a+2a_0\}/\min\{\sigma_4 a, \delta_4 a\}$. Figure 11(a),(b) indicates the $\lambda_2$ and $R$ for varying coupling strength $a$. Whatever the value of $a$ is, $\lambda_2$ decreases and $R$ increases gradually as time goes on. That is, the synchronizability weakens with time.

4) Variable coupling strength follows the logarithmic function

We take $\sigma_4 = \lg(t)$ (then $\delta_4 = (N\text{-}(\lg(t))\ \gamma\text{-}1)/(N\text{-}\gamma\text{-}1)$) for the numerical simulation. Then $\lambda_2 = \min$

$\{\sigma_4 a, \delta_4 a\}$, $R = \lambda_{max}/\lambda_2 = \max\{Md+\sigma_4 a+2a_0, Md+\delta_4 a+2a_0\}/\min\{\sigma_4 a, \delta_4 a\}$. Figure 12(a),(b) indicates the $\lambda_2$ and $R$ for varying coupling strength $a$. $\lambda_2$ gradually increases, then decreases as time goes on. $R$ gradually decreases, then increases slowly. That is, the synchronizability strengthens first and weakens with time.

5) Variable coupling strength follows the trigonometric function

We take $\sigma_5 = \sin t+1.5$ (then $\delta_4 = (N-(\sin t+1.5)\ \gamma-1)/(N-\gamma-1)$) for the numerical simulation. Then $\lambda_2 = \min\{\sigma_5 a, \delta_5 a\}$, $R = \lambda_{max}/\lambda_2 = \max\{Md+\sigma_5 a+2a_0, Md+\delta_5 a+2a_0\}/\min\{\sigma_5 a, \delta_5 a\}$. Figure 13(a),(b) indicates the $\lambda_2$ and $R$ for varying coupling strength $a$. We could find $\lambda_2$ and $R$ vary periodically.

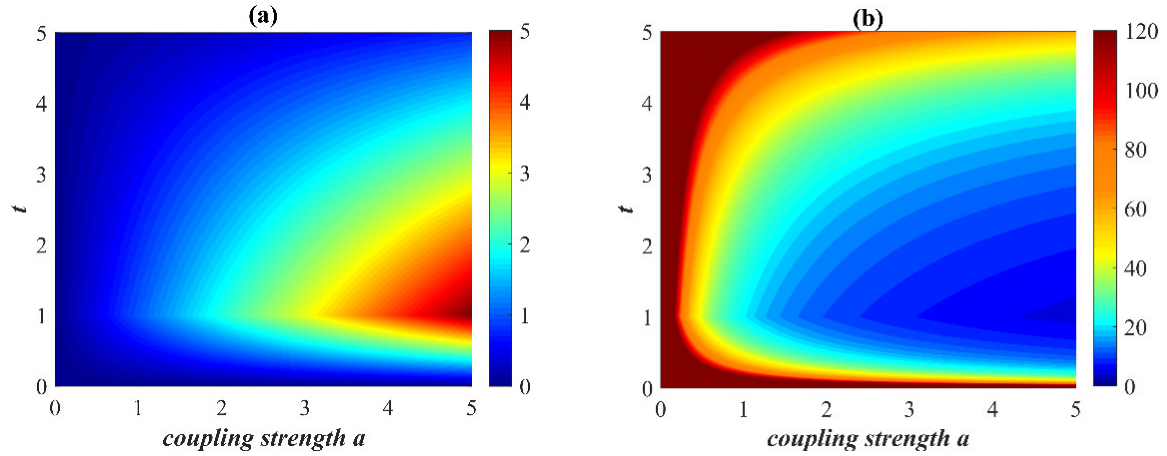


**Figure 9.** $\lambda_2$ and $R$ when the coupling strength varies as the proportional function.

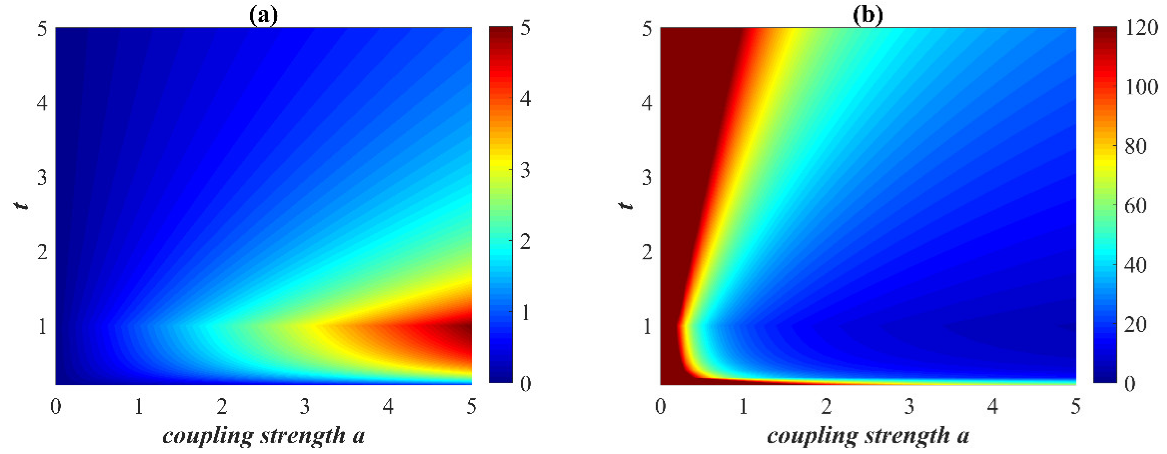


**Figure 10.** $\lambda_2$ and $R$ when the coupling strength varies as inverse proportional function.

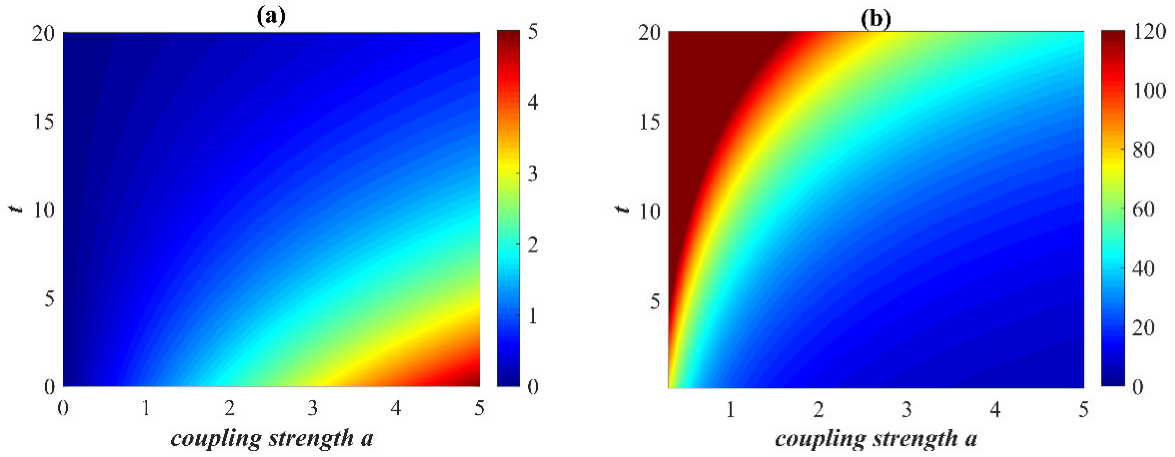


**Figure 11.** $\lambda_2$ and $R$ when the coupling strength varies as exponential function.

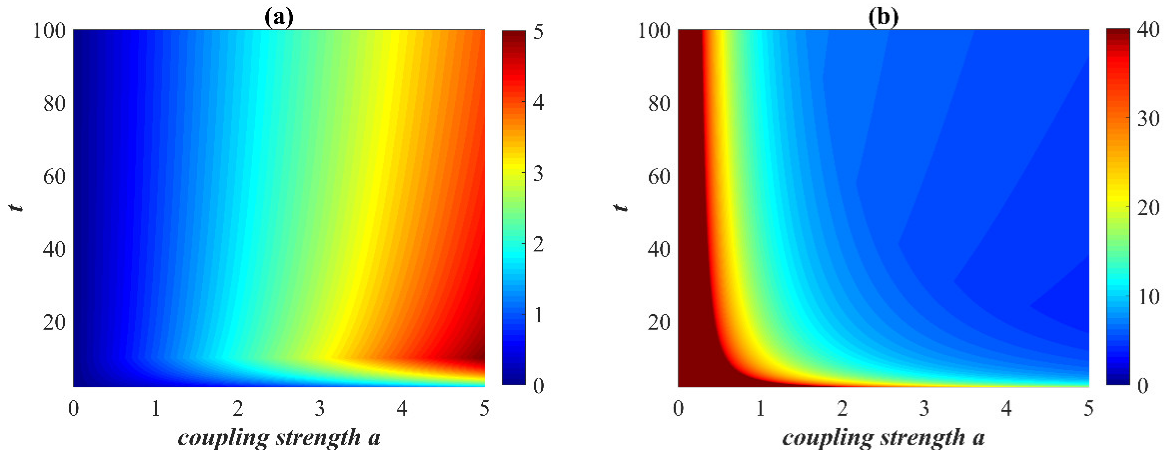


**Figure 12.** $\lambda_2$ and $R$ when the coupling strength varies as logarithmic function.

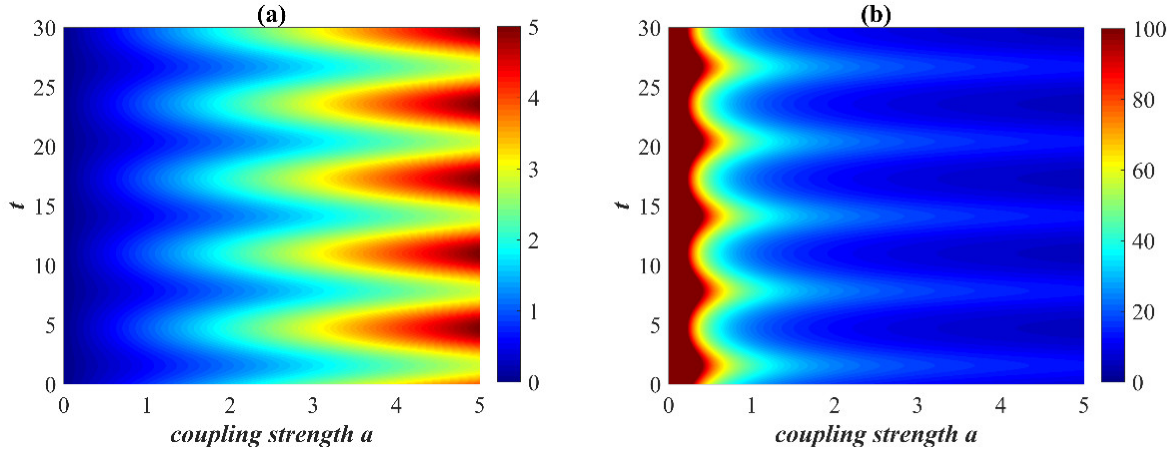


**Figure 13.** $\lambda_2$ and $R$ when the coupling strength varies as trigonometric function.

By comparing and analyzing Sections 3 and 4, the variable coupling strengths $\sigma a$ and $\delta a$ only have an impact on the divergent coupling star-ring network. Furthermore, the topological parameters of the network affect both coupling modes, whether the synchronous regions are bounded or unbounded.

## 5. Synchronization control

A detailed and rigorous theoretical derivation is presented for the eigenvalue spectrum and synchronizability of the star-ring network under different coupling cases in Sections 3 and 4. Based on the theoretical analysis, simulations are conducted to investigate the effect of different topological parameters on synchronizability. In this section, synchronization control experiments on multilayer star-ring networks will be performed to verify the above analytical results. For simplicity, consider a multilayer network with $M$ layers, each containing $N$ nodes, which is described by

$$\dot{\boldsymbol{x}}_i^K = f\left(\boldsymbol{x}_i^K(t)\right) + c^K \sum_{K=1}^{M}\sum_{j=1}^{N} a_{ij}^K \boldsymbol{H}_K \boldsymbol{x}_j^K(t) + p\sum_{Z=1}^{M} d_i^{(KZ)} \boldsymbol{\Gamma} \boldsymbol{x}_i^Z(t) + \boldsymbol{u}_i^K(t), \tag{8}$$

the relevant descriptions for Eq (8) are similar to Eq (1), $\boldsymbol{u}_i^K(t)$ is an adaptive controller particularly.

Assume the Hindmarsh-Rose [46,47] system is selected as the dynamic system described by:

$$\begin{cases} \dot{x} = y - ax^3 + bx^2 - z + I_{ext} \\ \dot{y} = c - dx^2 - y \\ \dot{z} = r\left(S\left(x - x_0\right) - z\right) \end{cases}, \tag{9}$$

where, $x$, $y$, and $z$ are defined as the membrane potential of the neuron, the recovery variable, and the slow-varying adaptive current of the neuron in the system, respectively. $a = 1$, $b = 3$, $c = 1$, $d = 5$, $r = 0.006$, $S = 4$, $x_0 = -1.56$, $I_{ext} = 3$. Its chaotic system and time history are shown in Figure 14.

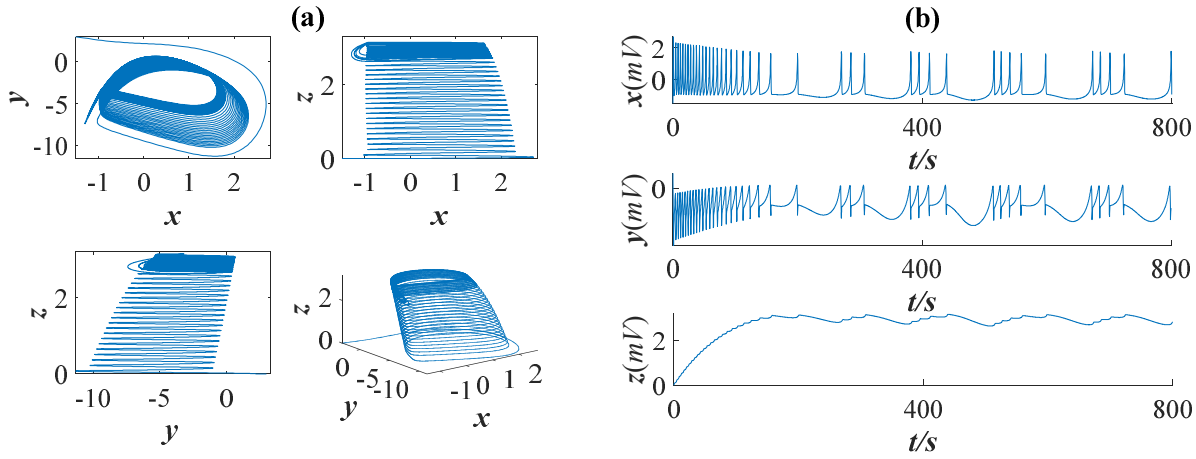


**Figure 14.** Hindmarsh-Rose system and time evolution of $x$, $y$, $z$.

The target system $\boldsymbol{s}(t)$ of the network is defined as follows:

$$\dot{\boldsymbol{s}}(t) = f\left(\boldsymbol{s}(t)\right), \tag{10}$$

then synchronization errors of the networks are defined as:

$$\boldsymbol{e}_i^K(t) = \boldsymbol{x}_i^K(t) - \boldsymbol{s}(t). \tag{11}$$

Subsequently, the error systems can be derived as follows:

$$\dot{\boldsymbol{e}}_i^K(t)=f\left(\boldsymbol{e}_i^K(t)+\boldsymbol{s}(t)\right)-f\left(\boldsymbol{s}(t)\right)+c^K\sum_{K=1}^{M}\sum_{j=1}^{N}a_{ij}^K\boldsymbol{H}_K\boldsymbol{e}_j^K(t)+p\sum_{Z=1}^{M}d_i^{(KZ)}\boldsymbol{\Gamma}\boldsymbol{e}_i^Z(t)+\boldsymbol{u}_i^K(t). \quad (12)$$

If $\lim_{t\to\infty}\|\boldsymbol{e}_i^K(t)\|=0$ is satisfied, it can be inferred that the multilayer complex networks and the target system have achieved synchronization. Designing an adaptive controller as follows:

$$\begin{cases}\boldsymbol{u}_i^K(t)=-d_i^K(t)\boldsymbol{H}_K\boldsymbol{e}_i^K(t)\\ \dot{d}_i^K(t)=h_i^K\left[\boldsymbol{e}_i^K(t)\right]^{\mathrm{T}}\boldsymbol{H}_K\boldsymbol{e}_i^K(t)\end{cases}, \quad (13)$$

where $h_i^K>0$ and $d_i^K(t)$ is the adaptive feedback control gains.

**Theorem 5.1.** *Based on Hypothesises 2.1 and 2.2, the error system is asymptotically synchronization under the controller, if there exists* $d^*>0$ *satisfying*

$$\left(\frac{\alpha^2+1}{2}+\kappa p\right)\boldsymbol{I}+\boldsymbol{\Psi}<0, \quad (14)$$

*where*,

$$\kappa=\max_{1\le i\le n}\left\{\lambda_{\max}\left(\boldsymbol{D}_i\boldsymbol{D}_i^{\mathrm{T}}\otimes\boldsymbol{\Gamma}\boldsymbol{\Gamma}^{\mathrm{T}}\right)\right\},\ \boldsymbol{D}_i=\begin{bmatrix}d_i^{(11)} & d_i^{(12)} & \cdots & d_i^{(1M)}\\ d_i^{(21)} & d_i^{(22)} & \cdots & d_i^{(2M)}\\ \vdots & \vdots & \ddots & \vdots\\ d_i^{(M1)} & d_i^{(11)} & \cdots & d_i^{(MM)}\end{bmatrix},$$

$$\boldsymbol{\Psi}=\begin{bmatrix}\left(c_K\dfrac{\boldsymbol{A}^{(1)}+\left(\boldsymbol{A}^{(1)}\right)^{\mathrm{T}}}{2}-d^*I_N\right)\otimes\boldsymbol{H}_K & & \\ & \ddots & \\ & & \left(c_K\dfrac{\boldsymbol{A}^{(M)}+\left(\boldsymbol{A}^{(M)}\right)^{\mathrm{T}}}{2}-d^*I_N\right)\otimes\boldsymbol{H}_K\end{bmatrix}.$$

***Proof.*** Consider the following Lyapunov-krasovskii [48] candidate as:

$$V(t)=\frac{1}{2}\sum_{K=1}^{M}\sum_{i=1}^{N}\left[\boldsymbol{e}_i^K(t)\right]^{\mathrm{T}}\boldsymbol{e}_i^K(t)+\frac{1}{2}\sum_{K=1}^{M}\sum_{i=1}^{N}\frac{1}{h_i^K}\left(d_i^K(t)-d^*\right)^2, \quad (15)$$

one gains

$$\begin{aligned}
\dot{V}(t) &= \sum_{K=1}^{M}\sum_{i=1}^{N}\left(\boldsymbol{e}_i^K(t)\right)^{\mathrm{T}}\left(f\left(\boldsymbol{x}_i^K(t)\right)-f\left(\boldsymbol{s}(t)\right)+\boldsymbol{u}_i^K(t)+c^K\sum_{j=1}^{N}a_{ij}^K\boldsymbol{H}_K\boldsymbol{e}_j^K(t)+p\sum_{Z=1}^{M}d_i^{(KZ)}\boldsymbol{\Gamma}\boldsymbol{e}_i^Z(t)\right)\\
&+\sum_{K=1}^{M}\sum_{i=1}^{N}\frac{1}{h_i^K}\left(d_i^K(t)-d^*\right)\dot{d}_i^K(t)\\
&=\sum_{K=1}^{M}\sum_{i=1}^{N}\left(\boldsymbol{e}_i^K(t)\right)^{\mathrm{T}}\left(f\left(\boldsymbol{e}_i^K(t)+\boldsymbol{s}(t)\right)-f\left(\boldsymbol{s}(t)\right)\right)+c^K\sum_{K=1}^{M}\sum_{i=1}^{N}\sum_{j=1}^{N}\left(\boldsymbol{e}_i^K(t)\right)^{\mathrm{T}}a_{ij}^K\boldsymbol{H}_K\boldsymbol{e}_j^K(t)\\
&+p\sum_{K=1}^{M}\sum_{Z=1}^{M}\sum_{i=1}^{N}\left(\boldsymbol{e}_i^K(t)\right)^{\mathrm{T}}d_i^{(KZ)}\boldsymbol{\Gamma}\boldsymbol{e}_i^Z(t)-d^*\sum_{K=1}^{M}\sum_{i=1}^{N}\left(\boldsymbol{e}_i^K(t)\right)^{\mathrm{T}}\boldsymbol{H}_K\boldsymbol{e}_i^K(t)\\
&=\frac{1}{2}\sum_{K=1}^{M}\left(\boldsymbol{e}^K(t)\right)^{\mathrm{T}}\boldsymbol{e}^K(t)+\frac{1}{2}\sum_{K=1}^{M}\left(f\left(\boldsymbol{e}^K(t)+\boldsymbol{s}(t)\right)-f\left(\boldsymbol{s}(t)\right)\right)^{\mathrm{T}}\left(f\left(\boldsymbol{e}^K(t)+\boldsymbol{s}(t)\right)-f\left(\boldsymbol{s}(t)\right)\right)\\
&+c^K\sum_{K=1}^{M}\left(\boldsymbol{e}^K(t)\right)^{\mathrm{T}}\left(\boldsymbol{A}^{(K)}\otimes\boldsymbol{H}_K\right)\boldsymbol{e}^K(t)+p\sum_{K=1}^{M}\sum_{Z=1}^{M}\sum_{i=1}^{N}d_i^{(KZ)}\left(\boldsymbol{e}^K(t)\right)^{\mathrm{T}}\boldsymbol{\Gamma}\boldsymbol{e}_i^Z(t)\\
&-d^*\sum_{K=1}^{M}\left(\boldsymbol{e}^K(t)\right)^{\mathrm{T}}\left(\boldsymbol{I}_N\otimes\boldsymbol{H}_K\right)\boldsymbol{e}^K(t),\\
&\le\frac{\alpha^2+1}{2}\sum_{K=1}^{M}\left(\boldsymbol{e}^K(t)\right)^{\mathrm{T}}\boldsymbol{e}^K(t)+\sum_{K=1}^{M}\left(\boldsymbol{e}^K(t)\right)^{\mathrm{T}}\left[\left(c^K\frac{\boldsymbol{A}^{(K)}+\left(\boldsymbol{A}^{(K)}\right)^{\mathrm{T}}}{2}-d^*\boldsymbol{I}_N\right)\otimes\boldsymbol{H}_K\right]\boldsymbol{e}^K(t)\\
&+p\lambda_{\max}\left(\frac{\boldsymbol{D}+\boldsymbol{D}^{\mathrm{T}}}{2}\otimes\boldsymbol{\Gamma}\right)\sum_{K=1}^{M}\sum_{Z=1}^{M}\left(\boldsymbol{e}^K(t)\right)^{\mathrm{T}}\boldsymbol{e}^Z(t)\\
&=\left[\left(\frac{\alpha^2+1}{2}+\kappa p\right)\boldsymbol{I}+\Psi\right]\boldsymbol{\beta}^{T}\boldsymbol{\beta}.
\end{aligned}\tag{16}$$

Where, $\boldsymbol{\beta}=((\boldsymbol{e}^{(1)}(t))^{\mathrm{T}},(\boldsymbol{e}^{(2)}(t))^{\mathrm{T}},\ldots,(\boldsymbol{e}^{(M)}(t))^{\mathrm{T}})^{\mathrm{T}}$. The error systems (16) are shown to achieve asymptotic synchronization by Theorem 5.1. Therefore, the proof is now completed.

**Remark 2.** *In addition to the theoretical derivation of synchronizability in [49], the synchronization control of the constructed multilayer star-ring network model is added. Precise synchronization control can be achieved by changing the size of the topological parameters correlated to synchronizability.*

In accordance with the master stability function theory, if the inner coupling continuous matrix Γ is an identity matrix, the synchronous region is unbounded. Therefore, the synchronizability of the network is determined by the λ2 of its Laplacian matrix [50]. We select a divergent directionally coupled star-ring network for simulation, and N is even. From Table 1, λ2 = Md. The following topological parameters of the multilayer star-ring network are selected for numerical simulation: N = 50, d0 = 1, a = 1, a0 = 1, d = 1 (when considering the variation of M), and M = 3 (when considering the variation of d). Figure 15 shows the synchronization errors ||e|| versus time. Figure 15 reveals that the synchronization speed increases with M, indicating greater synchronizability at higher M. From Figure 15(b), the speed of synchronization exhibits a gradual increase with d. Therefore, the synchronizability becomes stronger as d increases. Figure 16 shows the evolution of the error in each dimension of the node over time for different numbers of layers M. As the number of layers M increases,

it can clearly be seen that synchronizability improves. Figure 17 shows the variation of the error of each dimension node over time with d, and the results show that a larger d leads to faster synchronization.

Conclusive evidence is provided by the synchronization control experiments in this section, confirming the validity of the synchronizability analysis results. As the network structure becomes larger, leading to an increase in synchronizability. Additionally, the strength of interlayer coupling also enhances synchronizability. Consequently, it is possible to effectively implement control by determining the key topology parameters that have a correlation with synchronizability.

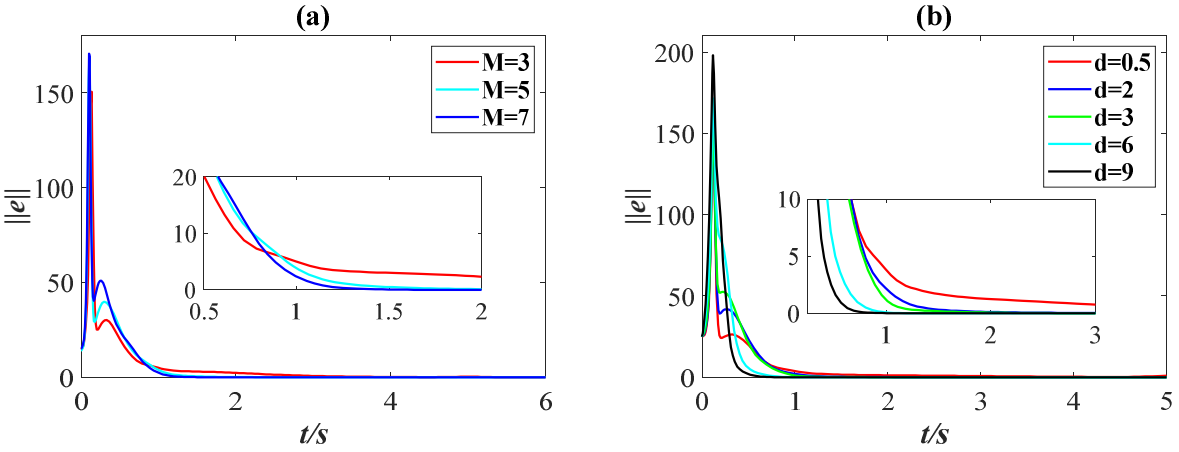


**Figure 15.** The synchronization errors $\|\boldsymbol{e}\|$ of the multilayer divergent coupled star-ring networks evolve with time.

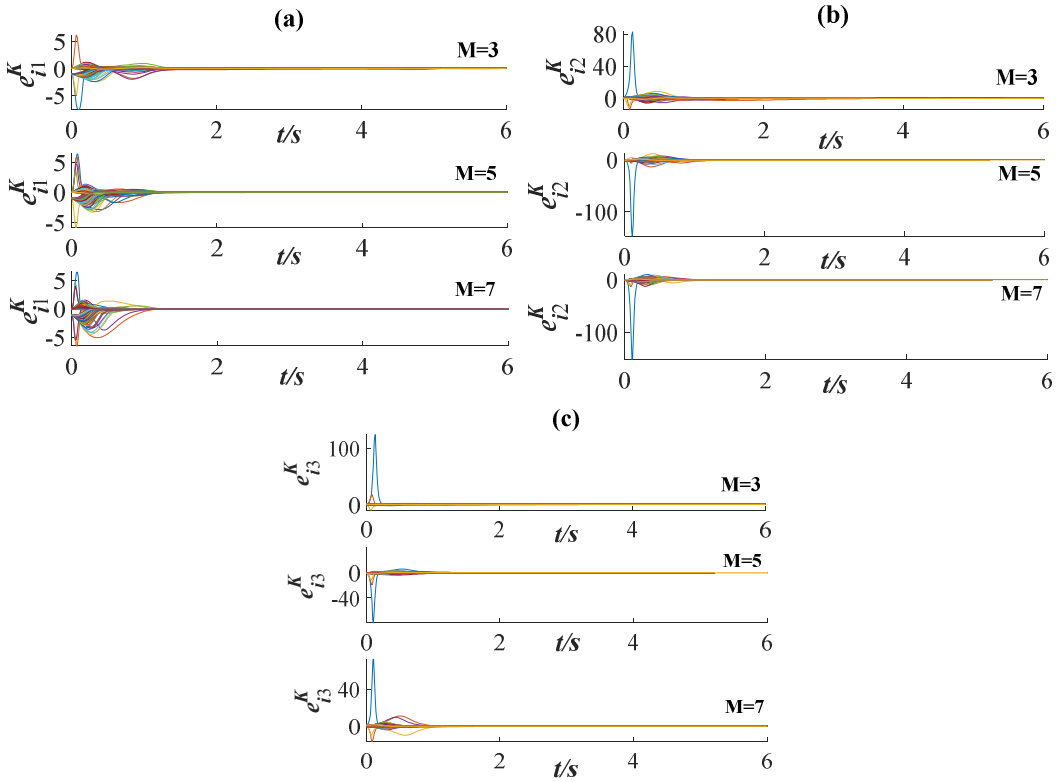


**Figure 16.** The errors $\boldsymbol{e}_{in}^{K}(t)$ ($n$ = 1, 2, 3, $M$ = 3 ($i$ = 1, 2 ,…, 150, $K$ = 1, 2, 3), $M$ = 5($i$ = 1, 2,…, 250, $K$ = 1, 2, ..,5), $M$ = 7($i$ = 1, 2, …, 350, $K$ = 1, 2, …, 7)) evolve with time.

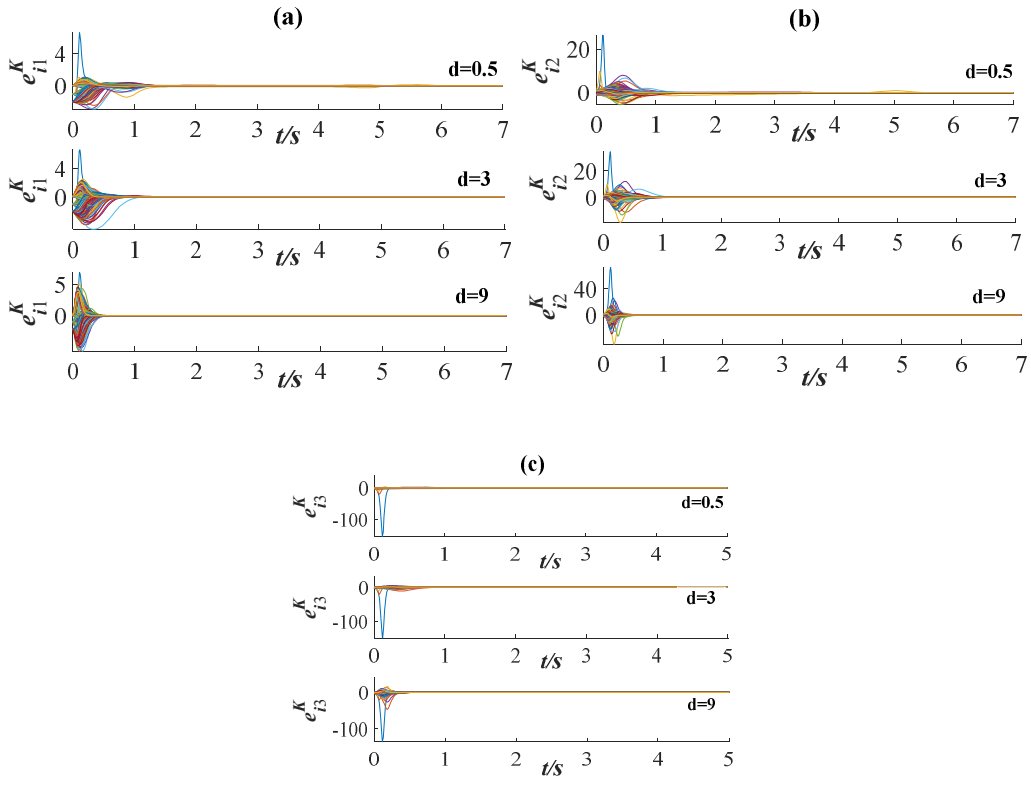


**Figure 17.** The errors $e_{in}^{K}(t)$ ($n$ = 1, 2, 3, $I$ =1, 2, …, 150, $K$ = 1, 2, 3) evolve with time under different $d$.

## 6. Conclusions and discussion

The eigenvalue spectrum of the supra-Laplacian matrix of multilayer star-ring networks is rigorously derived in this paper, considering divergent and aggregated coupling within the subnetwork. Compared with Sections 3 and 4, when the synchronized regions are bounded and unbounded, the variable coupled strengths $\sigma a$ and $\delta a$ are closely connected to the synchronizability of the aggregated coupling but have no correlation with the divergent coupling. Synchronizability is firmly related to the topological parameters, including the number of nodes $N$, intralayer coupling strengths $a$ and $a_0$, interlayer coupling strengths $d$ and $d_0$, and the number of layers $M$ in the divergent coupling model. In the case of an unbounded synchronous region, when $N$ is odd, it is primarily influenced by the topological parameter $a_0$. A bounded synchronous region depends on several factors, including $N$, $a$, $a_0$, $d_0$, and $M$. In addition, when $N$ is even, $M$ and $d$ are relevant to the synchronizability with the unbounded synchronous region. When $N$ is even, it is determined by $N$, $a$, $d_0$, $d$, and $M$ with the bounded synchronous region. Particularly, the synchronizability is significantly related to the intralayer variable coupling strengths $\sigma a$ and $\delta a$ with aggregated coupling. When $\sigma$ changes with different functions, the tendency toward synchronizability is found. Finally, a numerical simulation of a star-ring network composed of the Hindmarsh-Rose systems is given to verify the validity of the synchronizability analysis.

Based on the research on multilayer star-ring networks in this paper, coupling mode, coupling strength and topological parameters play an important role in the analysis of synchronizability. Through the analysis of synchronizability and the synchronization process, it has some theoretical reference value for understanding and exploring practical problems in engineering. In particular, adjusting traffic network signals, optimizing control in the Internet of Things and improving

communication network transmission efficiency can give a certain theoretical perspective. So far, there are still many unsolved problems related to multilayer networks. There is a requirement for further research, as there are various theoretical and practical issues that need to be addressed and overcome.

## Use of AI tools declaration

The authors declare they have not used Artificial Intelligence (AI) tools in the creation of this article.

## Acknowledgments

This work is supported by the National Natural Science Foundation of China (Nos. 11602146, 11872304), the Science Foundation of Shanghai (No. 18ZR1438200), and the Chen Guang Project supported by the Shanghai Municipal Education Commission and Shanghai Education Development Foundation (No. 16CG65). Xia Tan is supported by National Natural Science Foundation of China (No. 12102266).

## Conflict of interest

The authors declare there is no conflict of interest.

## References

1. R. Albert, A. L. Barabási, Statistical mechanics of complex networks, *Rev. Mod. Phys.*, **74** (2002), 47–97. https://doi.org/10.1103/RevModPhys.74.47
2. A. L. Barabasi, Z. N. Oltvai, Network biology: understanding the cell's functional organization, *Nat. Rev. Genet.*, **5** (2004), 101–113. https://doi.org/10.1038/nrg1272
3. M. E. J. Newman, Communities, modules and large-scale structure in networks, *Nat. Phys.*, **8** (2012), 25–31. https://doi.org/10.1038/nphys2162
4. J. Lin, Y. Ban, Complex network topology of transportation systems, *Transport Rev.*, **33** (2013), 658–685. https://doi.org/10.1080/01441647.2013.848955
5. R. E. Mirollo, S. H. Strogatz, Synchronization of pulse-coupled biological oscillators, *SIAM J. Appl. Math.*, **50** (1990), 1645–1662. https://doi.org/10.1137/0150098
6. X. Zhang, S. Boccaletti, S. Guan, Z. Liu, Explosive synchronization in adaptive and multilayer networks, *Phys. Rev. Lett.*, **114** (2015), 038701. https://doi.org/10.1103/PhysRevLett.114.038701
7. P. Wang, G. Wen, X. Yu, W. Yu, T. Huang, Synchronization of multi-layer networks: from node-to-node synchronization to complete synchronization, *IEEE Trans. Circuits Syst. I Regul. Pap.*, **66** (2018), 1141–1152. https://doi.org/10.1109/TCSI.2018.2877414
8. H. Liu, Y. Li, Z. Li, J. Lü, J. Lu, Topology identification of multilink complex dynamical networks via adaptive observers incorporating chaotic exosignals, *IEEE Trans. Cybern.*, **52** (2022), 6255–6268. https://doi.org/10.1109/TCYB.2020.3042223
9. G. Mei, X. Wu, Y. Wang, M. Hu, J. Lu, G. Chen, Compressive-sensing-based structure identification for multilayer networks, *IEEE Trans. Cybern.*, **48** (2017), 754–764. https://doi.org/10.1109/TCYB.2017.2655511

10. X. Wang, A. Tejedor, Y. Wang, Y. Moreno, Unique superdiffusion induced by directionality in multiplex networks, *New J. Phys.*, **23** (2021), 013016. https://doi.org/10.1088/1367-2630/abdb71
11. M. Turalska, K. Burghardt, M. Rohden, A. Swami, R. M. D'Souza, Cascading failures in scale-free interdependent networks, *Phys. Rev. E: Stat. Nonlinear Soft Matter Phys.*, **99** (2019), 032308. https://doi.org/10.1103/PhysRevE.99.032308
12. J. Chang, X. Yin, C. Ma, D. Zhao, Y. Sun, Estimation of the time cost with pinning control for stochastic complex networks, *Electron. Res. Arch.*, **30** (2022), 3509–3526. https://doi.org/10.3934/era.2022179
13. S. S. Sajjadi, D. Baleanu, A. Jajarmi, H. M. Pirouz, A new adaptive synchronization and hyperchaos control of a biological snap oscillator, *Chaos, Solitons Fractals*, **138** (2020), 109919. https://doi.org/10.1016/j.chaos.2020.109919
14. S. Liu, R. Zhang, Q. Wang, X. He, Sliding mode synchronization between uncertain Watts-Strogatz small-world spatiotemporal networks, *Appl. Math. Mech.*, **41** (2020), 1833–1846. https://doi.org/10.1007/s10483-020-2686-6
15. K. Hengster-Movric, K. You, F. L. Lewis, L. Xie, Synchronization of discrete-time multi-agent systems on graphs using Riccati design, *Automatica*, **49** (2013), 414–423. https://doi.org/10.1016/j.automatica.2012.11.038
16. L. M. Pecora, T. L. Carrollton, Synchronization in chaotic systems, *Phys. Rev. Lett.*, **64** (1990), 821–827. https://doi.org/10.1103/PhysRevLett.64.821
17. Z. Wu, X. Fu, Complex projective synchronization in drive-response networks coupled with complex-variable chaotic systems, *Nonlinear Dyn.*, **72** (2013), 9–15. https://doi.org/10.1007/s11071-012-0685-7
18. H. Hong, M. Y. Choi, B. J. Kim, Synchronization on small-world networks, *Phys. Rev. E: Stat. Nonlinear Soft Matter Phys.*, **65** (2002), 026139. https://doi.org/10.1103/PhysRevE.65.026139
19. K. Li, S. Guan, X. Gong, C. H. Lai, Synchronization stability of general complex dynamical networks with time-varying delays, *Phys. Lett. A*, **372** (2008), 7133–7139. https://doi.org/10.1016/j.physleta.2008.10.054
20. X. Zhao, J. Zhou, J. Lu, Pinning synchronization of multiplex delayed networks with stochastic perturbations, *IEEE Trans. Cybern.*, **49** (2018), 4262–4270. https://doi.org/10.1109/TCYB.2018.2861822
21. A. Fan, J. Li, J. Li, Adaptive event-triggered prescribed performance learning synchronization for complex dynamical networks with unknown time-varying coupling strength, *Nonlinear Dyn.*, **100** (2020), 2575–2593. https://doi.org/10.1007/s11071-020-05648-w
22. S. Gomez, A. Diaz-Guilera, J. Gomez-Gardenes, C. J. Pérez-Vicente, Y. Moreno, A. Arenas, Diffusion dynamics on multiplex networks, *Phys. Rev. Lett.*, **110** (2013), 028701. https://doi.org/10.1103/PhysRevLett.110.028701
23. J. A. Almendral, A. Díaz-Guilera, Dynamical and spectral properties of complex networks, *New J. Phys.*, **9** (2007), 187. https://doi.org/10.1088/1367-2630/9/6/187
24. C. Granell, S. Gómez, A. Arenas, Dynamical interplay between awareness and epidemic spreading in multiplex networks, *Phys. Rev. Lett.*, **111** (2013), 128701. https://doi.org/10.1103/PhysRevLett.111.128701
25. J. Aguirre, R. Sevilla-Escoboza, R. Gutierrez, D. Papo, M. Buldú, Synchronization of interconnected networks: the role of connector nodes, *Phys. Rev. Lett.*, **112** (2014), 248701. https://doi.org/10.1103/PhysRevLett.112.248701

26. M. Xu, J. Lu, J. Zhou, Synchronizability and eigenvalues of two-layer star networks (in Chinese), *Acta Phys. Sin.*, **65** (2016), 028902. https://doi.org/10.7498/aps.65.028902
27. J. Li, Y. Luan, X. Wu, J. Lu, Synchronizability of double-layer dumbbell networks, *Chaos*, **31** (2021), 073101. https://doi.org/10.1063/5.0049281
28. Y. Deng, Z. Jia, F. Yang, Synchronizability of multilayer star and star-ring networks, *Discrete Dyn. Nat. Soc.*, **2020** (2020), 9143917. https://doi.org/10.1155/2020/9143917
29. P. Peng, J. Wang, K. Huang, Reliable fiber sensor system with star-ring-bus architecture, *Sensors*, **10** (2010), 4194–4205. https://doi.org/10.3390/s100504194
30. C. Christodoulou, G. Ellinas, Resilient architecture for optical access networks, *Photonic Network Commun.*, **41** (2021), 1–16. https://doi.org/10.1007/s11107-020-00910-y
31. S. Liu, L. Chen, Second-order terminal sliding mode control for networks synchronization, *Nonlinear Dyn.*, **79** (2015), 205–213. https://doi.org/10.1007/s11071-014-1657-x
32. R. Li, H. Wu, J. Cao, Exponential synchronization for variable-order fractional discontinuous complex dynamical networks with short memory via impulsive control, *Neural Networks*, **148** (2022), 13–22. https://doi.org/10.1016/j.neunet.2021.12.021
33. Y. Tang, F. Qian, H. Gao, J. Kurths, Synchronization in complex networks and its application–a survey of recent advances and challenges, *Annu. Rev. Control*, **38** (2014), 184–198. https://doi.org/10.1016/j.arcontrol.2014.09.003
34. Y. Shi, Y. Ma, Finite/fixed-time synchronization for complex networks via quantized adaptive control, *Electron. Res. Arch.*, **29** (2021), 2047–2061. https://doi.org/10.3934/era.2020104
35. Z. Qin, J. Wang, Y. Huang, S. Ren, Analysis and adaptive control for robust synchronization and $H_\infty$ synchronization of complex dynamical networks with multiple time-delays, *Neurocomputing*, **289** (2018), 241–251. https://doi.org/10.1016/j.neucom.2018.02.031
36. A. Zentani, N. Zulkifli, A. Ramli, Network resiliency and fiber usage of Tree, Star, ring and wheel based wavelength division multiplexed passive optical network Topologies: a comparative review, *Opt. Fiber Technol.*, **73** (2022), 103038. https://doi.org/10.1016/j.yofte.2022.103038
37. M. Xu, K. An, L. H. Vu, Z. Ye, J. Feng, E. Chen, Optimizing multi-agent based urban traffic signal control system, *J. Intell. Transp. Syst.*, **23** (2019), 357–369. https://doi.org/10.1080/15472450.2018.1501273
38. L. Xing, Cascading failures in internet of things: review and perspectives on reliability and resilience, *IEEE Internet Things J.*, **8** (2020), 44–64. https://doi.org/10.1109/JIOT.2020.3018687
39. J. Wei, X. Wu, J. Lu, X. Wei, Synchronizability of duplex regular networks, *EuroPhys. Lett.*, **120** (2018), 20005. https://doi.org/10.1209/0295-5075/120/20005
40. L. Tang, X. Wu, J. Lü, J. Lu, R. M. D'Souza, Master stability functions for complete, intralayer, and interlayer synchronization in multiplex networks of coupled Rössler oscillators, *Phys. Rev. E: Stat. Nonlinear Soft Matter Phys.*, **99** (2019), 012304. https://doi.org/10.1103/PhysRevE.99.012304
41. L. M. Pecora, T. L. Carroll, Master stability functions for synchronized coupled systems, *Phys. Rev. Lett.*, **80** (1998), 2109. https://doi.org/10.1103/PhysRevLett.80.2109
42. J. Sun, X. Li, J. Zhang, Y. Shen, Y. Li, Synchronizability and eigenvalues of multilayer star networks through unidirectionally coupling (in Chinese), *Acta Phys. Sin.*, **66** (2017), 188901. https://doi.org/10.7498/aps.66.188901

43. X. Jin, Z. Wang, H. Yang, Q. Song, M. Xiao, Synchronization of multiplex networks with stochastic perturbations via pinning adaptive control, *J. Franklin Inst.*, **358** (2021), 3994–4012. https://doi.org/10.1016/j.jfranklin.2021.03.004
44. X. Mao, A note on the LaSalle-type theorems for stochastic differential delay equations, *J. Math. Anal. Appl.*, **268** (2002), 125–142. https://doi.org/10.1006/jmaa.2001.7803
45. F. Yang, Z. Jia, Y. Deng, Eigenvalue spectrum and synchronizability of two types of double-layer star-ring networks with hybrid directional coupling, *Discrete Dyn. Nat. Soc.*, **2021** (2021), 1–20. https://doi.org/10.1155/2021/6623648
46. J. L. Hindmarsh, R. M. Rose, A model of the nerve impulse using two first-order differential equations, *Nature*, **296** (1982), 162–164. https://doi.org/10.1038/296162a0
47. L. Xu, G. Qi, J. Ma, Modeling of memristor-based Hindmarsh-Rose neuron and its dynamical analyses using energy method, *Appl. Math. Modell.*, **101** (2022), 503–516. https://doi.org/10.1016/j.apm.2021.09.003
48. L. Shi, C. Zhang, S. Zhong, Synchronization of singular complex networks with time-varying delay via pinning control and linear feedback control, *Chaos, Solitons Fractals*, **145** (2021), 110805. https://doi.org/10.1016/j.chaos.2021.110805.
49. Y. Deng, Z. Jia, G. Deng, Q. Zhang, Eigenvalue spectrum and synchronizability of multiplex chain networks, *Physica A*, **537** (2020), 122631. https://doi.org/10.1016/j.physa.2019.122631
50. Y. Li, X. Wu, J. Lu, J. Lü, Synchronizability of duplex networks, *IEEE Trans. Circuits Syst. II Express Briefs*, **63** (2015), 206–210. https://doi.org/10.1109/TCSII.2015.2468924



AIMS Press